Journal of Alloys and Compounds 771 (2019) 762–768

Contents lists available at ScienceDirect

Journal of Alloys and Compounds

journal homepage: http://www.elsevier.com/locate/jalcom

Structural evolution and electronic properties of Cu-Zn alloy clusters

Qiman Liu [a], Longjiu Cheng [a, b, *]

[a] Department of Chemistry, Anhui University, Hefei, Anhui, 230601, PR China
[b] Anhui Province Key Laboratory of Chemistry for Inorganic/Organic Hybrid Functionalized Materials, Hefei, Anhui, 230601, PR China

ARTICLE INFO

Article history:
Received 9 February 2018
Received in revised form
2 August 2018
Accepted 3 August 2018
Available online 6 August 2018

Keywords:
Superatom
Chemical bonding
Structural prediction
Brass
Nanoalloy

ABSTRACT

Brass (Cu-Zn) is one of the typical Hume-Rothery alloys, which is extensively used in material science and industry. Earlier studies revealed that the structures of Cu-Zn alloys correlate with the average number of valence electrons or the electron-per-atom (e/a) ratio, but structural evolution rule still remains unclear. In this work, the Cu-Zn nanoalloy clusters (elementary cells of bulk brass) are studied to reveal the evolutional rule of their structures with sizes. Systematic unbiased global search is performed for structural prediction of Cu_xZn_y nanoalloys in a size range ($x + y = 3–10$) by using genetic algorithm with density functional theory. The global minimum and low-lying isomers of the series of nanoalloy clusters are obtained, and the structural phase diagrams are plotted depending on the relative energy. The results show that geometric structures of Cu-Zn nanoalloys are also determined by the total number of valence electrons (n^*), just as in bulk brass. Cu-Zn nanoalloys with same n^* have similar geometric motifs. When $n^* = 6$, the clusters adopt planar motif, which have σ-aromaticity following the $(4n+2)$ rule. When $n^* = 8$, 18 and 20, the clusters keep spherical motifs, which satisfy the magic numbers of Jellium model and could be viewed as stable superatoms. In most of cases for $n^* = 10$, 12 and 14, the clusters adopt prolate motifs, which have similar electronic structures to N_2, O_2, and F_2 molecules, respectively, based on the super valence bond model. Moreover, in some cases for $n^* = 10$ and 12, the clusters can be seen as an 8e-superatom combined with one (8e+2e) or two (8e+2e+2e) separate Zn atoms.

1. Introduction

Brass (Cu-Zn) is one of the oldest and most common alloys, of which the phase stability mechanisms are decided by the electronic effects [1–6]. The difference between the structures of brass is interesting as the structural transformation occurs when one half of the Cu atoms are replaced by Zn, which has one extra electron as compared to Cu. On the Cu-rich side with low valence electron to atom ratio (e/a) of the phase diagram, a face-centered-cubic (fcc) solid solution is stable. On the Zn-rich side, there is a series of partially ordered phases [7–10]. However, the structural description of solid solutions is complicated. Brass Cu_5Zn_8 is the most common example, which is treated as an assembly of 26-atom nested polyhedral cluster composed of four interpenetrating icosahedra [11,12].

Properties of the alloys could be improved by structural adjustment at nanoscale. Reducing the particle size is one of the effective ways, and it has been the hot subject of nanotechnology studies in recent years. By now, a mixture of different phases of brass nanoparticles including α, β, γ and ε has been obtained by several fabrication methods [13–17]. Recently, Jagirdar et al. prepared Cu/Zn@Cu core-shell nanocomposites and demonstrated a structural evolution of various Cu-Zn bimetallic nanophases starting from bulk brass [15]. Although a number of experimental studies of bulk brass have been reported, there are little studies on brass alloys with the atomic-scale structures. Thus, exploring the structural transformation rule connected with different compositions in Cu-Zn clusters makes a great sense.

There have been a number of theoretical reports devoted to bimetallic clusters. For instance, Johnston et al. [18] obtained the structures of the global minima (GM) for eight atom bimetallic CuAg and CuAu neutral clusters using a genetic algorithm (GA) approach at the density functional theory (DFT) level. Yoshiyuki and co-workers [19] reported a high-spin icosahedral ground state for $Al_{12}Cu$ in accordance with the Hund's rule of maximum spin at half-filling. Soon after that, the $Al_{12}Cu$ superatom as a stable

* Corresponding author. Department of Chemistry, Anhui University, Hefei, Anhui, 230601, PR China.
E-mail address: clj@ustc.edu (L. Cheng).

https://doi.org/10.1016/j.jallcom.2018.08.033
0925-8388/

building block for ionic salts was reported [20]. Kiwi et al. studied structural and electronic properties of 13-atom Ag-Au nanoalloys using DFT method, focusing on their 2D to 3D structural transformation [21]. In addition, a series of 13-atom Cu-Zn nanoalloy clusters was also studied by DFT calculations, and the results indicate that structures of copper rich clusters tend to be compact, often icosahedral, whereas zinc rich clusters have compact copper cores surrounded by an incomplete shell of solvated Zn atoms [22].

Metal clusters with a certain number of valence electrons exhibit high electronic and structural stability owing to a specific electronic shell filling rule - just as simple atoms, which were regarded as superatoms by Jena and Khana [23–26]. The superatom model has been successfully used in explaining the stability of metal clusters with closed-shell electronic structure [19,27–30]. However, the superatom model is based on a spherical field associated with spherical cluster motifs, so it cannot be used to explain the shell orders of non-spherical clusters. In 2013, the super valence bond (SVB) [31] and the superatom network (SAN) [32] concepts were proposed by Cheng and Yang. In SVB model, a non-spherical metallic cluster can be viewed as a superatomic molecule composed by spherical superatoms via sharing atomic nuclei and valence electrons [33–35]. More recently, a quintuple super bond between superatoms of metallic clusters was reported based on the SVB model [36].

Here we started our explorations of the size-dependent growth behavior of the bimetallic Cu_xZn_y ($x + y = 3–10$) nanoalloys related to their geometric and electronic properties. Due to the huge number of local minima (each one corresponding to a possible cluster structure) and homotops (isomers with the same geometry and composition, but with a different arrangement of the two types of atoms), binary clusters present a complex potential energy surface (PES) [37–40]. Therefore, we scan the PES of the clusters by using GA with DFT, to gain the most reliable structures of Cu-Zn systems. Our results show great diversity and flexibility in geometric and electronic structures for Cu-Zn binary clusters. The electronic stability and chemical bonding patterns are also discussed in this work.

2. Computational details

The GM and low-energy structures of Cu_xZn_y ($x + y = 3–10$) nanoalloy clusters are located by the combination of GA and DFT methods, which were successfully applied to structural predictions of a number of cluster systems [18,41–43]. GAs belong to a large class of evolutionary algorithms, which generate solutions to optimization problems using techniques inspired by natural evolution, such as inheritance, mutation, selection, and crossover [44,45]. In this work, more than 1000 samplings are optimized by DFT at each constitution. In global research of the PES, a small basis set (LANL2DZ) [46] is used for saving time. After global optimization, the low-lying candidates are fully relaxed at the BP86-D3/def2-TZVP [47,48] level of theory, and the frequencies are also calculated at this level to ensure that they belong to true local minima. Energies of the structures reported herein include the contribution of zero point energy (ZPE) corrections. Furthermore, the adaptive natural density partitioning (AdNDP) [49,50] method is used to study the chemical bonding of Cu-Zn clusters. All quantum chemical calculations are performed with the Gaussian 09 [51] suite of programs and molecular orbital visualization is performed by Molekel 5.4.

To verify the reliability of the DFT methods used in this work, a benchmark calculation is carried out by comparing relative stability of the four low-energy isomers of Cu_4Zn_1 cluster calculated in different methods. Table 1 gives the results of the benchmark calculation for DFT/def2-TZVP and CCSD(T)/def2-QZVPP. It can be seen that, gaps of the relative energies for the four Cu_4Zn_1 isomers optimized in BP86-D3 functional are in good agreement with those in CCSD(T) method. Accuracy of the DFT functionals was also checked by the calculated bond length of Cu_2 dimer. As listed in Table 2, the calculated bond length in BP86-D3 functional is 2.25 Å, in good agreement with the experimental value (2.22 Å). Moreover, the calculated binding energy of Cu_2 dimer at BP86-D3/def2-TZVP (48.60 *k*cal/mol) is also in good agreement with the experimental value (47.9 *k*cal/mol) [52], indicating high reliability of the computational method.

Table 1
Comparison of single point energies for the four low-lying isomers of Cu_4Zn_1 (see structures in Fig. S1).[a]

Method	4-1I	4-1II	4-1III	4-1IV
CCSD(T)	−8336.282225	0.152	0.150	0.184
TPSSH	−8341.581246	0.125	0.193	0.158
TPSS	−8341.732135	0.104	0.178	0.177
TPSS-D3	−8341.743943	0.069	0.180	0.176
PBE0	−8340.332750	0.205	0.187	0.142
PBE0-D3	−8340.341312	0.180	0.187	0.141
B3LYP	−8341.818048	0.351	0.147	0.190
B3LYP-D3	−8341.836823	0.279	0.150	0.190
M06	−8341.399938	0.240	0.110	0.261
M062x	−8341.311138	0.312	0.147	0.182
BP86	−8342.903033	0.230	0.154	0.196
BP86-D3	−8342.922754	0.166	0.160	0.196
B97D3	−8345.547746	0.291	0.141	0.187
PBE	−8340.361718	0.188	0.160	0.183

[a] Energies for 4-1I are in atomic units, while other energies are relative to this in eV.

3. Results and discussion

The GM and low-energy isomers of Cu_xZn_y ($x + y = 3–10$) nanoclusters are fully relaxed at the BP86-D3/def2-TZVP level of theory, which are given in Figs. S1 and S2 in the Supporting Information. All isomers are verified to be true local minima by frequency check. Bare Cu_n and Zn_n clusters have been explored by DFT method in literatures [53–56], and all the predicted structures are reproduced in this work.

3.1. Geometric structures and structural phase diagrams

To give a direct view of the structural evolution of the Cu-Zn binary systems, the structural phase diagrams (SPDs) are plotted in Fig. 1 and Fig. 2, presenting information of stability *versus* composition. To give a reasonable measure of stability of the Cu_xZn_y clusters, the relative energy (E_{rel}) is calculated by taking Cu_2 molecule and Zn atom as references:

Table 2
Bond lengths (in Å) of Cu-Cu dimer.

Dimer	Bond lengths (Å)
Cu-Cu	2.25[a], 2.26[b], 2.28[c], 2.27[d], 2.41[e], 2.26[f], 2.25[g], 2.29[h], 2.31[i], 2.22[j]

[a] TPSS.
[b] TPSSH.
[c] PBE0.
[d] PBE.
[e] M062x.
[f] M06.
[g] BP86-D3.
[h] B3LYP.
[i] CCSD(T).
[j] Exp.

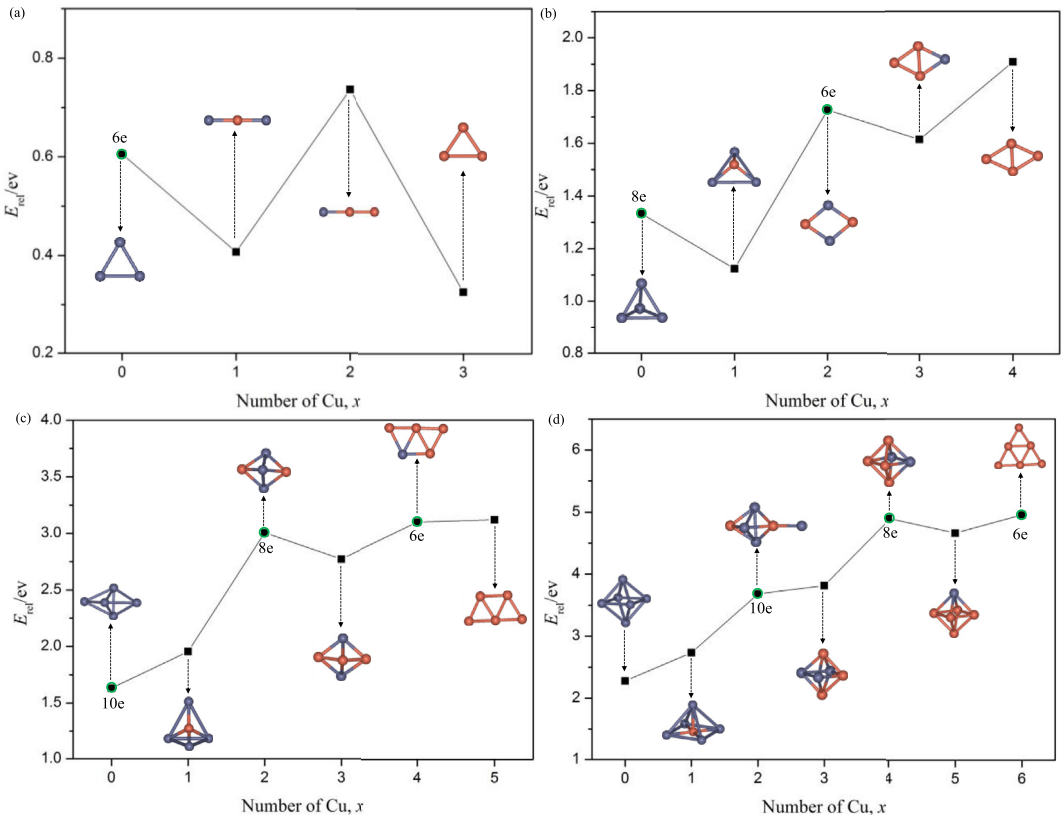

Fig. 1. Structural phase diagrams (SPDs) of Cu_xZn_y ($x + y = 3–6$) clusters. The GM structures are also labeled.

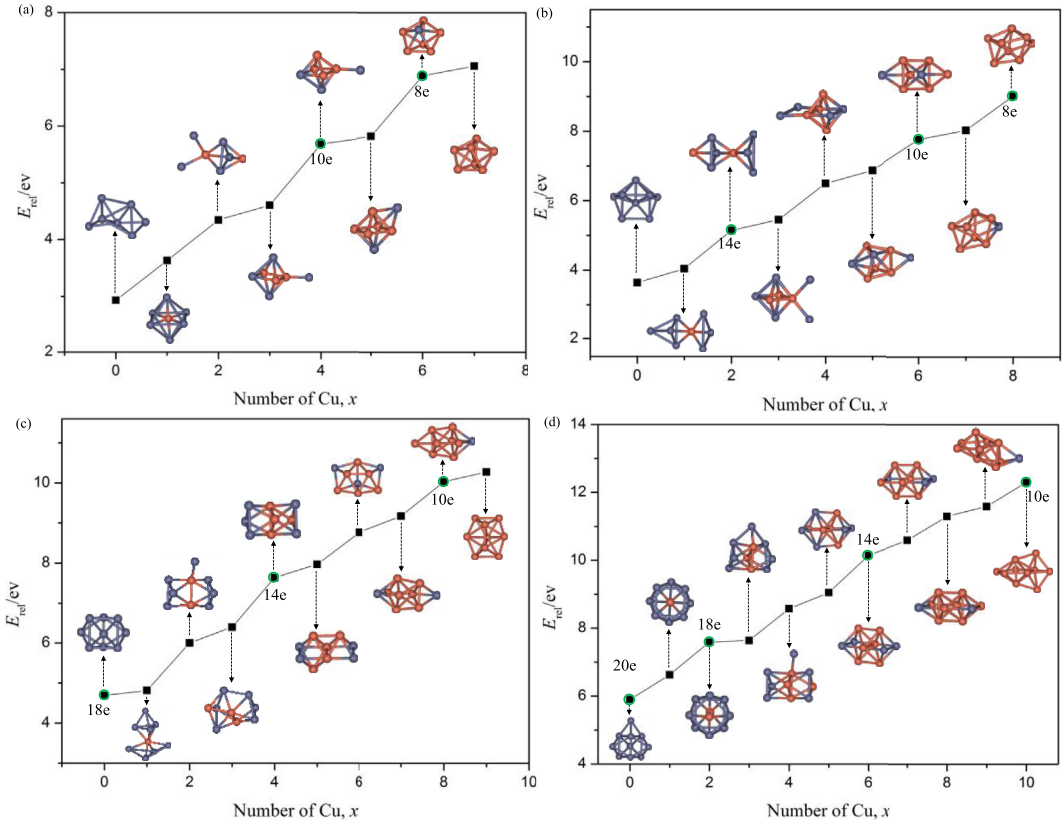

Fig. 2. Structural phase diagrams (SPDs) of Cu_xZn_y ($x + y = 7–10$) clusters. The GM structures are also labeled.

$$E_{rel} = E(Cu_xZn_y) - xE(Cu_2)/2 - yE(Zn),$$

wherein $E(Cu_xZn_y)$, $E(Cu_2)$ and $E(Zn)$ are energies of Cu_xZn_y, Cu_2 molecule and Zn atom, respectively. Here we take Cu_2 molecule as the reference instead of Cu atom, because Cu atom has half-filled $4s^1$ orbital and usually has higher binding energy than Zn atoms ($4s^2$). The magnitude of E_{rel} represents relative stability of the cluster, that is, a cluster with greater positive E_{rel} is more stable. E_{rel} is a key indicator for stability of a Cu-Zn cluster, and is useful to compare the relative stability of Cu-Zn clusters at different compositions. The peaks of E_{rel} correspond to particularly stable structures, which are labeled by green circles in the figures. The GM structures are also labeled in the SPDs.

Fig. 1a plots the SPD of the trimers, which is quite simple. Zn_3 has an equilateral triangle structure with D_{3h} symmetry. Cu_3 also has a triangle structure, but the symmetry is C_{2v} due to the Jahn-Teller effect. Cu_1Zn_2 and Cu_2Zn_1 are both linear structures.

Fig. 1b plots the SPD of the 4-atom clusters. Zn_4 with 8 valence electrons is a tetrahedron with T_d symmetry. Cu_2Zn_2 has a tetragonal planar structure with D_{2h} symmetry. Cu_3Zn_1 and Cu_4 are also planar structures.

Fig. 1c plots the SPD of the 5-atom clusters. Zn_5 is a trigonal bipyramid with D_{3h} symmetry. Cu_2Zn_3 cluster exhibits a spherical structure, owing to a specific electronic shell filling. The planar structure of Cu_4Zn_1 can be obtained via doping Cu_5 with Zn atom.

Fig. 1d plots the SPD of the 6-atom clusters. Zn_6, Cu_3Zn_3, Cu_4Zn_2 and Cu_5Zn_1 are octahedral structures. Cu_1Zn_5 is a pentagonal pyramidal structure with one central Cu atom. The irregular structure of Cu_2Zn_4 is composed of a compact spherical Cu_2Zn_3 and a separate Zn atom.

Fig. 2a plots the SPD of the 7-atom clusters. Zn_7 is a trigonal bipyramid with C_2 symmetry. There is a 6-atom octahedron unit in Cu_1Zn_6, Cu_3Zn_4, Cu_4Zn_3 and Cu_5Zn_2. Cu_2Zn_5 can be considered as one compact spherical structure plus two separate Zn atoms. Cu_6Zn_1 and Cu_7 are pentagonal bipyramids.

Fig. 2b plots the SPD of the 8-atom clusters. Cu_1Zn_7 and Cu_2Zn_6 adopt similar motifs, where Cu atoms have a high coordination. The structural frameworks of Cu_6Zn_2, Cu_4Zn_4 and Cu_3Zn_5 are based on the 6-atoms octahedra, while Cu_5Zn_3 is based on the pentagonal bipyramid Cu_7 structure. The capped octahedron of Cu_7Zn_1 can be obtained via doping Cu_8 with one Zn atom.

Fig. 2c plots the SPD of the 9-atom clusters. Zn_9 with 18 valence electrons is a tricapped trigonal prism with D_{3h} symmetry. Cu_4Zn_5 is a prolate body-fused bi-octahedron. For Cu_5Zn_3, Cu_7Zn_2 and Cu_8Zn_1, the structures are based on 6-atoms octahedra. Cu_9 is a prolate structure with C_{2v} symmetry.

Fig. 2d plots the SPD of the 10-atom clusters. Zn_{10} is a square antiprism with C_{3v} symmetry, which can be obtained by capping one Zn atom on Zn_9. Cu_1Zn_9 and Cu_2Zn_8 are cage structures. For Cu_9Zn_1 and Cu_{10}, the structures are based on the pentagonal bipyramid Cu_7 cluster. Furthermore, the body-fused bi-octahedron also appears in Cu_5Zn_5, Cu_6Zn_4, Cu_7Zn_3 and Cu_8Zn_2 clusters.

Overall, small-sized Cu clusters favor planar structures, whereas bimetallic Cu-Zn and pure Zn clusters prefer 3D structures. The Cu-rich clusters tend to have compact geometries, and Cu atoms show a trend to settle in a high-coordination site. Moreover, there are obviously odd-even behaviors in the SPDs, indicating that the clusters with even-numbered electrons are more stable.

3.2. Electronic structures

As shown in the SPDs, Cu-Zn nanoalloy clusters with the same number of valence electrons (n^*) usually have similar geometries despite their different compositions, of which the ones with certain n^* number (as labeled by green circles in the SPDs) exhibit high stability. In order to reach understanding of this phenomenon, we focus on the electronic characteristics and bonding features of these clusters.

3.2.1. 6e compounds

As shown in Fig. 3, in the case of $n^* = 6$, all the clusters (Zn_3, Cu_2Zn_2, Cu_4Zn_1 and Cu_6) are in planar motifs. Chemical bonding

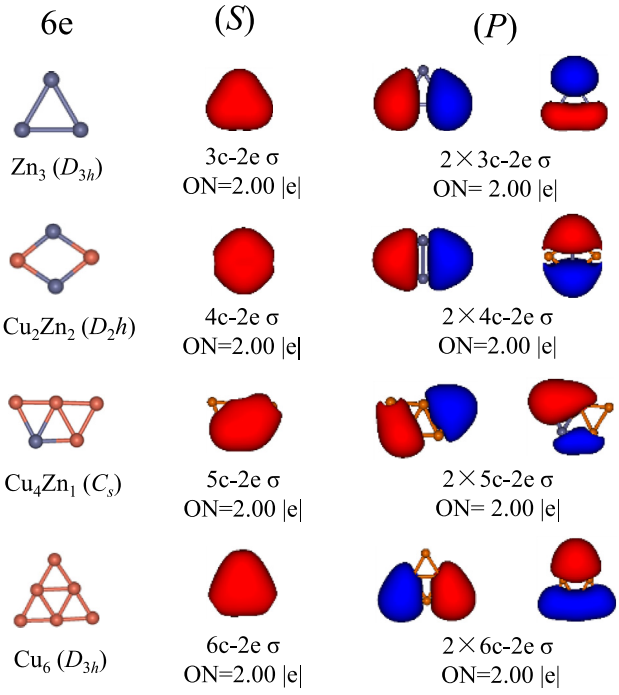

Fig. 3. Structures and AdNDP localized natural bonding orbitals of the 6e (Zn_3, Cu_2Zn_2, Cu_4Zn_1 and Cu_6) clusters.

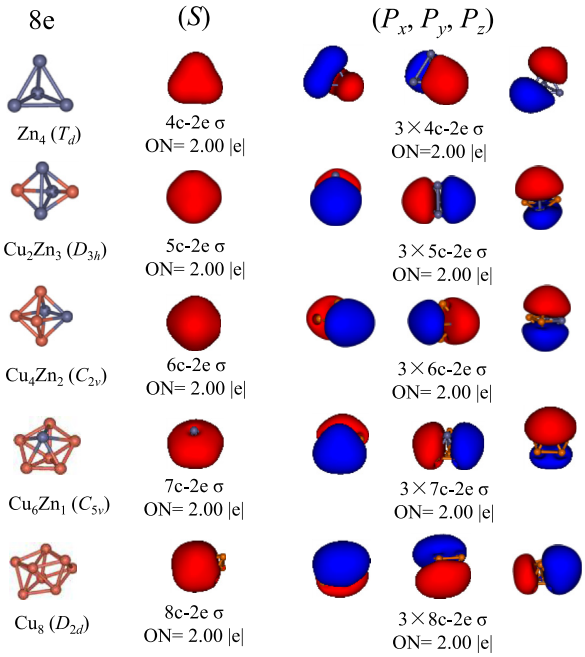

Fig. 4. Structures and AdNDP localized natural bonding orbitals of the 8e (Zn_4, Cu_2Zn_3, Cu_4Zn_2, Cu_6Zn_1 and Cu_8) clusters.

analysis by AdNDP reveals that Zn_3 cluster has three 3c-2e σ-bonds with occupancy number ON = 2.00 |e|. The occupation number represents the number of electrons involved in a bond. This indicates that the six valence electrons are delocalized over the three-atomic cycle, which is responsible for σ-aromaticity satisfying Hückel's 4*n*+2 rule. Similarly, Cu_2Zn_2, Cu_4Zn_1, and Cu_6 have three 4c-2e, 5c-2e, and 6c-2e σ-bonds (ON = 2.00|e|), respectively. Thus, each cluster forms closed-shell electronic structure following 6-electron principle to make it stable.

3.2.2. 8e compounds

Fig. 4 plots the spherical structures of Zn_4, Cu_2Zn_3, Cu_4Zn_2, Cu_6Zn_1 and Cu_8 clusters. They are eight-electron clusters satisfying the magic number in Jellium model. AdNDP analysis reveals that Zn_4 cluster has four delocalized 4c-2e σ-bonds, which can be clearly viewed as one super *S*-type lone pair (LP) orbital and three super *P*-type LP orbitals. Thus, Zn_4 cluster has a completely filled superatomic shell (SP^3), and can be considered as a stable spherical superatom. The electronic structures of Cu_2Zn_3, Cu_4Zn_2, Cu_6Zn_1 and Cu_8 are also similar (SP^3).

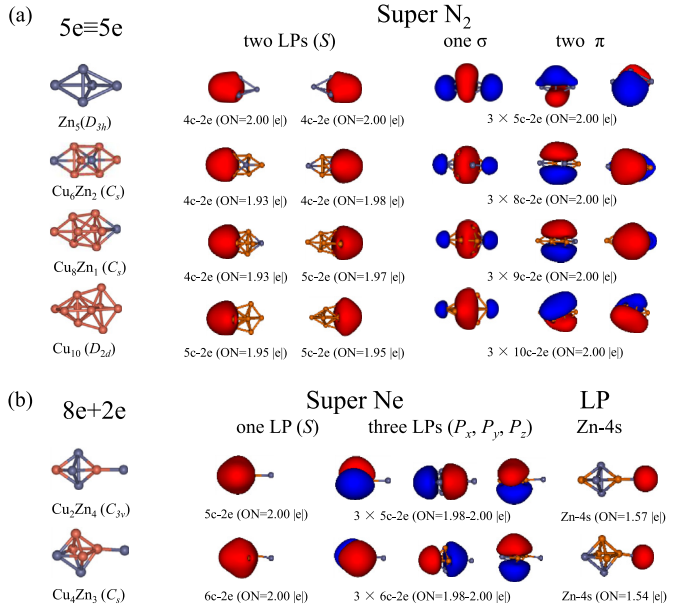

Fig. 5. Structures and AdNDP localized natural bonding orbitals of the 10e clusters: (a) Zn_5, Cu_6Zn_2, Cu_8Zn_1 and Cu_{10}; (b) Cu_2Zn_4 and Cu_4Zn_3.

3.2.3. 10e compounds

There are two different types of motifs for the 10e compounds. Zn_5, Cu_6Zn_2, Cu_8Zn_1 and Cu_{10} are prolate structures. Based on the SVB model of superatomic molecule, a prolate cluster can be seen as an integration of two spherical superatoms sharing valence pairs. As shown in Fig. 5a, Zn_5 can be seen as an integration of two 4c-5e spherical superatoms sharing three Zn atoms. AdNDP analysis reveals one 4c-2e super LP in each superatom with occupancy number ON = 2.00 |e| (*S*), one 5c-2e super σ-bond (ON = 2.00 |e|), and two 5c-2e super π-bonds (ON = 2.00 |e|), which resembles N_2 molecule in bonding frameworks. The situations in Cu_6Zn_2, Cu_8Zn_1 and Cu_{10} are also similar.

However, as shown in Fig. 5b, Cu_2Zn_4 and Cu_4Zn_3 are spherical compact structures linked to one separate Zn atom. Chemical bonding analysis by AdNDP reveals that Cu_2Zn_4 cluster has four 5c-2e super LPs (SP^3), and one 4s-LP for the separate Zn atom with occupancy number ON = 1.57 |e|. The situation in Cu_4Zn_3 is also similar, which can be seen as a 6c-8e spherical superatom connected to one separate Zn atom. The interaction between the 8e superatom and the separate Zn atom is non-bonding, which can be verified by the binding energy. It should be noted that the calculated binding energies of Cu_2Zn_3-Zn and Cu_4Zn_2-Zn are only 0.66 eV and 0.77 eV, respectively, much lower than the calculated binding energy of Cu_2 (2.11 eV).

3.2.4. 12e compounds

Similar to the 10e compounds, Fig. 6 also shows two different motifs for the 12e compounds. Cu_6Zn_3 and Cu_8Zn_2 adopt prolate structures. AdNDP analysis shows that Cu_6Zn_3 has four 6c-2e super LPs, one 10c-2e super σ-bond, and one 10c-2e super π-bond, which is similar to the singlet O_2 molecule in bonding framework. Cu_8Zn_2 cluster has four 6c-2e super LPs, one 10c-2e super σ-bond, and one 10c-2e super π-bond. Such a bonding framework also shows that

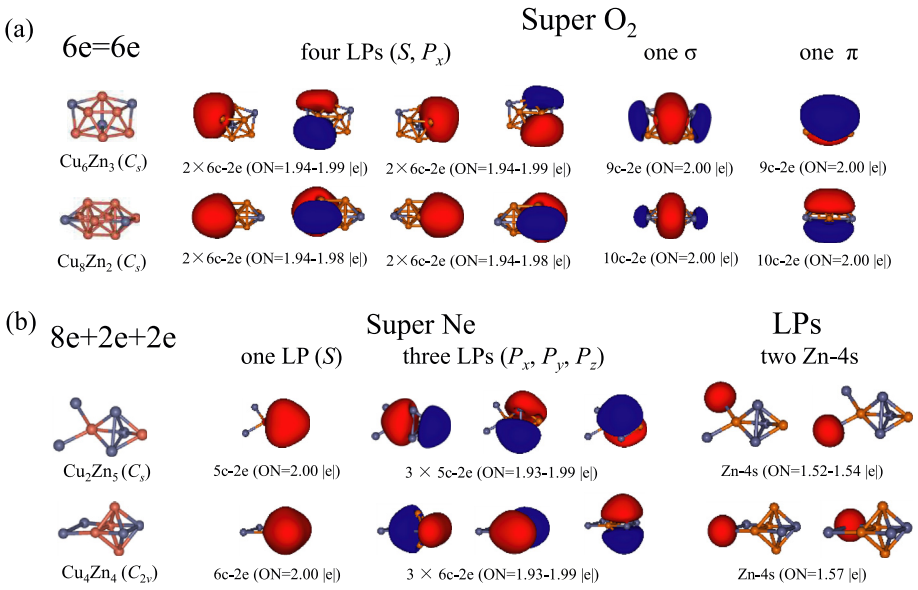

Fig. 6. Structures and AdNDP localized natural bonding orbitals of the 12e clusters. (a) Cu_6Zn_3, and Cu_8Zn_2; (b) Cu_2Zn_5 and Cu_4Zn_4.

Cu_8Zn_2 can be viewed as a superatomic molecule from the electronic structure point of view.

For Cu_2Zn_4 and Cu_4Zn_3, each cluster is composed of a spherical compact structure plus two separate Zn atoms. AdNDP analysis reveals that Cu_2Zn_5 has four 5c-2e super LPs (SP^3) and two Zn-4s LPs (ON = 1.52–1.54|e|). Similarly, there are four 6c-2e super LPs (SP^3) and two Zn-4s LPs (ON = 1.57|e|) in Cu_4Zn_4. This indicates that the electronic structures of Cu_2Zn_5 and Cu_4Zn_4 can be viewed as an 8e superatom connected to two separate Zn atoms.

3.2.5. 14e compounds

Fig. 7 plots the structures and chemical bonding patterns of the 14e (Zn_7, Cu_2Zn_6, Cu_4Zn_5 and Cu_6Zn_4) clusters, which adopt prolate motifs. According to the SVB model, the bonding frameworks of 14e compounds are similar to F_2 molecule. AdNDP analysis shows that, the 14 electrons of Zn_7 are delocalized in both tetrahedral superatoms, including two S-type super LPs, four P-type super LPs, and one super σ-bond. Similar bonding features have also been identified in Cu_2Zn_6, Cu_4Zn_5 and Cu_6Zn_4 clusters.

3.2.6. 18e and 20e compounds

The 18e (Zn_9 and Cu_2Zn_8) and 20e (Zn_{10}) are cage clusters with high symmetries, which are in electronic shell-closure following the Jellium model. Fig. 8 plots the molecular orbital (MO) diagrams of the three clusters. For the 18e compounds, the lowest MO has 1S character, and the next three MOs exhibit dominant 1P character, then followed by five typical 1D orbitals. Thus, e electronic shells of the 18e compounds are $(1S)^2(1P)^6(1D)^{10}$. Similarly, electronic shells of the 20e Zn_{10} cluster are $(1S)^2(1P)^6(1D)^{10}(2S)^2$. Each cluster has completely filled shells, which is consistent with the magic species of Jellium model.

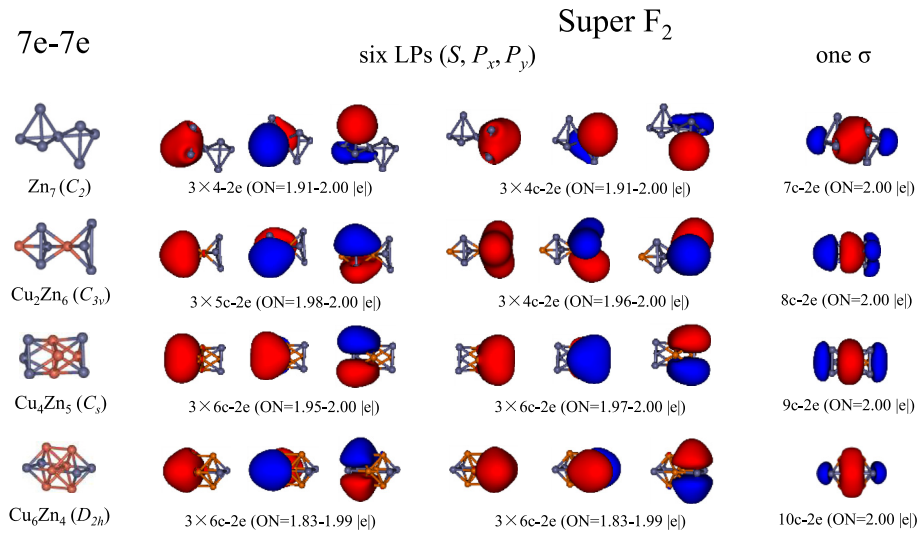

Fig. 7. Structures and AdNDP localized natural bonding orbitals of the 14e (Zn_7, Cu_2Zn_6, Cu_4Zn_5, and Cu_6Zn_4) clusters.

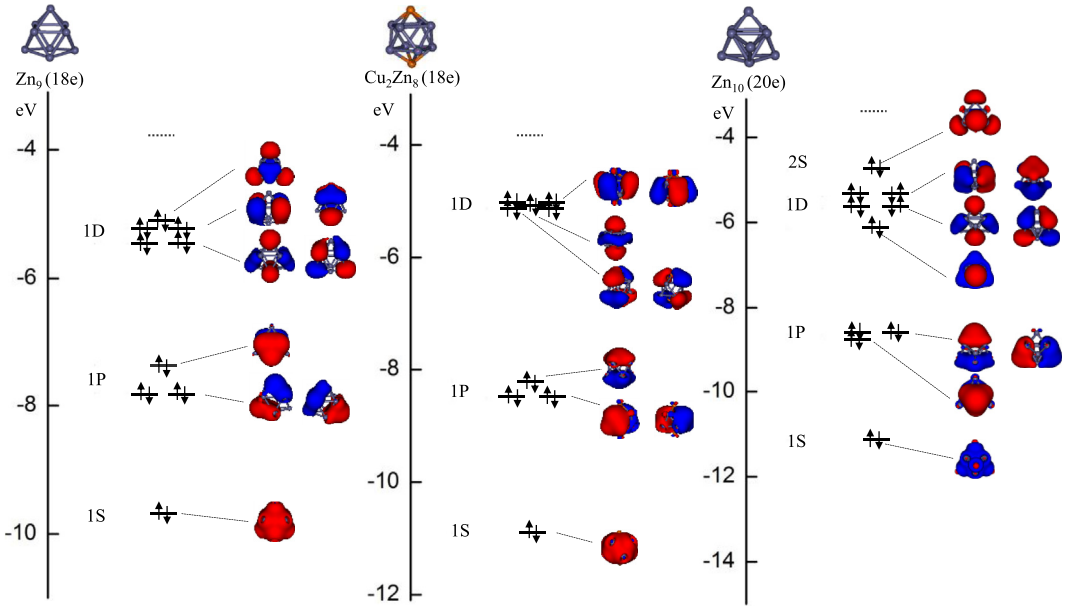

Fig. 8. Structures and the MO diagrams of the 18e (Zn_9 and Cu_2Zn_8) and 20e (Zn_{10}) clusters.

4. Conclusions

In summary, GM and low-energy structures of Cu_xZn_y nanoalloy clusters in a size range ($x + y = 3–10$) were located by using the GA-DFT method. The located structures were fully relaxed at the BP86-D3/Def2-TZVP level of theory, where the DFT method was verified to be reliable by benchmark calculations. The SPDs were given to investigate structural evolution of the nanoalloy clusters. It was found that the structures of Cu-Zn nanoalloy clusters are determined by their total number of valence electrons, and clusters with even valence electron numbers are more stable. The 6e compounds (Zn_3, Cu_2Zn_2, Cu_4Zn_1 and Cu_6) have planar motifs, and each cluster has three delocalized σ-bonds following the Huckel rule of planar aromaticity. The 8e compounds (Zn_4, Cu_2Zn_3, Cu_4Zn_2, Cu_6Zn_1 and Cu_8) have spherical compact structures, and AdNDP analysis reveals four delocalized σ-bonds in accordance with the superatom model. The 10e compounds have two different bonding features. One (Zn_5, Cu_6Zn_2, Cu_8Zn_1 and Cu_{10}) resembles N_2 molecule in electronic structures, and the other (Cu_2Zn_4 and Cu_4Zn_3) can be viewed as an 8e superatom (Ne) connected to one separate Zn atom. The 14e compounds (Zn_7, Cu_2Zn_6, Cu_4Zn_5 and Cu_6Zn_4) have prolate structures, which resemble F_2 molecule in bonding frameworks. Furthermore, the 18e and 20e compounds (Zn_9, Cu_2Zn_8 and Zn_{10}) are proved to be stable superatoms by MO diagrams following the Jellium model.

Bulk brass exhibit peculiar nested icosahedral structures. According to the electronic structures of the Cu-Zn nanoalloy clusters, the basic icosahedral units in bulk brass could be viewed as superatoms. Thus, it could be inferred that these superatomic crystals should be composed of icosahedral superatoms through super valence bond. Our study could give references for further studies on cluster-assembling materials and make sense in nanomaterial science.

Acknowledgements

This work is financed by the National Natural Science Foundation of China (21573001), and by the Foundation of Distinguished Young Scientists of Anhui Province. The calculations were carried out at the High-Performance Computing Center of Anhui University.

Appendix A. Supplementary data

Supplementary data related to this article can be found at https://doi.org/10.1016/j.jallcom.2018.08.033.

References

[1] S. Müller, A. Zunger, Phys. Rev. B 63 (2001), 094204.
[2] G.K. Wertheim, M. Campagna, S. Hüfner, Phys. Condens. Matter 18 (1974) 133–139.
[3] P.E. Turchi, M. Sluiter, F.J. Pinski, D.D. Johnson, D.M. Nicholson, G.M. Stocks, J.B. Staunton, Phys. Rev. Lett. 67 (1991) 1779–1782.
[4] R.F. Berger, P.L. Walters, S. Lee, R. Hoffmann, Chem. Rev. 111 (2011) 4522–4545.
[5] K. Freitag, H. Banh, C. Gemel, R.W. Seidel, S. Kahlal, J.Y. Saillard, R.A. Fischer, Chem. Commun. 50 (2014) 8681–8684.
[6] R. Ferrando, J. Jellinek, R.L. Johnston, Chem. Rev. 108 (2008) 845–910.
[7] S.N. Khan, M. Eisenbach, Phys. Rev. B 93 (2016), 024203.
[8] V.J. Keast, J. Ewald, K.S.B. De Silva, M.B. Cortie, B. Monnier, D. Cuskelly, E.H. Kisi, J. Alloys Compd. 647 (2015) 129–135.
[9] R.S. Dhaka, S. Banik, A.K. Shukla, V. Vyas, A. Chakrabarti, S.R. Barman, B.L. Ahuja, B.K. Sharma, Phys. Rev. B 78 (2008).
[10] V.F. Degtyareva, O. Degtyareva, M.K. Sakharov, N.I. Novokhatskaya, P. Dera, H.K. Mao, R.J. Hemley, J. Phys. Condens. Matter 17 (2005) 7955.
[11] A.A. Pankova, V.A. Blatov, G.D. Ilyushin, D.M. Proserpio, Inorg. Chem. 52 (2013) 13094–13107.
[12] O. Gourdon, D. Gout, D.J. Williams, T. Proffen, S. Hobbs, G.J. Miller, Inorg. Chem. 46 (2007) 251–260.
[13] M. Farbod, A. Mohammadian, Intermetallics 45 (2014) 1–4.
[14] K. Schutte, H. Meyer, C. Gemel, J. Barthel, R.A. Fischer, C. Janiak, Nanoscale 6 (2014) 3116–3126.
[15] S.P. Bhaskar, B.R. Jagirdar, J. Alloys Compd. 694 (2017) 581–595.
[16] R.E. Cable, R.E. Schaak, Chem. Mater. 19 (2007) 4098–4104.
[17] S.K. Pabi, J. Joardar, B.S. Murty, J. Mater. Sci. 31 (1996) 3207–3211.
[18] C.J. Heard, R.L. Johnston, Eur. Phys. J. D 67 (2013).
[19] V. Kumar, Y. Kawazoe, Phys. Rev. B 64 (2001), 115405.
[20] J.U. Reveles, T. Baruah, R.R. Zope, J. Phys. Chem. C 119 (2015) 5129–5137.
[21] F. Munoz, A. Varas, J. Rogan, J.A. Valdivia, M. Kiwi, Phys. Chem. Chem. Phys. 17 (2015) 30492–30498.
[22] J. Botticelli, R. Fournier, M. Zhang, Theor. Chem. Acc. 120 (2008) 583–589.
[23] W.D. Knight, K. Clemenger, W.A. de Heer, W.A. Saunders, M.Y. Chou, M.L. Cohen, Phys. Rev. Lett. 52 (1984) 2141–2143.
[24] W.A. de Heer, Rev. Mod. Phys. 65 (1993) 611–676.
[25] S.N. Khanna, P. Jena, Phys. Rev. Lett. 69 (1992) 1664–1667.
[26] A. Munoz-Castro, R. Arratia-Perez, Phys. Chem. Chem. Phys. 14 (2012) 1408–1411.
[27] A.C. Reber, S.N. Khanna, Acc. Chem. Res. 50 (2017) 255–263.
[28] D. Schebarchov, N. Gaston, Phys. Chem. Chem. Phys. 14 (2012) 9912–9922.
[29] R. Dong, X. Chen, H. Zhao, X. Wang, H. Shu, Z. Ding, L. Wei, Phys. Chem. Chem. Phys. 13 (2011) 3274–3280.
[30] Z. Luo, A.W. Castleman, Acc. Chem. Res. 47 (2014) 2931–2940.
[31] L. Cheng, J. Yang, J. Chem. Phys. 138 (2013) 141101.
[32] L. Cheng, Y. Yuan, X. Zhang, J. Yang, Angew. Chem. Int. Ed. 52 (2013) 9035–9039.
[33] L. Liu, P. Li, L. Yuan, L. Cheng, J. Yang, Nanoscale 8 (2016) 12787–12792.
[34] L. Cheng, X. Zhang, B. Jin, J. Yang, Nanoscale 6 (2014) 12440–12444.
[35] L. Liu, J. Yuan, L. Cheng, J. Yang, Nanoscale 9 (2017) 856–861.
[36] H. Wang, L. Cheng, Nanoscale 9 (2017) 13209–13213.
[37] L.O. Paz-Borbon, A. Gupta, R.L. Johnston, J. Mater. Chem. 18 (2008) 4154–4164.
[38] R. Ferrando, A. Fortunelli, R.L. Johnston, Phys. Chem. Chem. Phys. 10 (2008) 640–649.
[39] X. Wu, Y. Dong, New J. Chem. 38 (2014) 4893–4900.
[40] I. Demiroglu, K. Yao, H.A. Hussein, R.L. Johnston, J. Phys. Chem. C 121 (2017) 10773–10780.
[41] W. Liu, L. Cheng, J. Phys. Chem. C 120 (2016) 2432–2438.
[42] Z. Tian, L. Cheng, Phys. Chem. Chem. Phys. 17 (2015) 13421–13428.
[43] L. Cheng, J. Chem. Phys. 136 (2012) 104301.
[44] R.L. Johnston, Dalton Trans. (2003) 4193–4207.
[45] B. Hartke, J. Phys. Chem. 97 (1993) 9973–9976.
[46] P.J. Hay, W.R. Wadt, J. Chem. Phys. 82 (1985) 299–310.
[47] F. Weigend, R. Ahlrichs, Phys. Chem. Chem. Phys. 7 (2005) 3297–3305.
[48] J.P. Perdew, Phys. Rev. B 33 (1986) 8822–8824.
[49] D.Y. Zubarev, A.I. Boldyrev, Phys. Chem. Chem. Phys. 10 (2008) 5207–5217.
[50] T.R. Galeev, B.D. Dunnington, J.R. Schmidt, A.I. Boldyrev, Phys. Chem. Chem. Phys. 15 (2013) 5022–5029.
[51] M.J. Frisch, G.W. Trucks, H.B. Schlegel, G.E. Scuseria, J.R.C.M.A. Robb, G. Scalmani, V. Barone, B. Mennucci, H.N.G.A. Petersson, M. Caricato, X. Li, H.P. Hratchian, J.B.A.F. Izmaylov, G. Zheng, J.L. Sonnenberg, M. Hada, K.T.M. Ehara, R. Fukuda, J. Hasegawa, M. Ishida, T. Nakajima, O.K.Y. Honda, H. Nakai, T. Vreven, J.A. Montgomery Jr., F.O.J.E. Peralta, M. Bearpark, J.J. Heyd, E. Brothers, V.N.S.K.N. Kudin, T. Keith, R. Kobayashi, J. Normand, A.R.K. Raghavachari, J.C. Burant, S.S. Iyengar, J. Tomasi, N.R.M. Cossi, J.M. Millam, M. Klene, J.E. Knox, J.B. Cross, C.A.V. Bakken, J. Jaramillo, R. Gomperts, R.E. Stratmann, A.J.A.O. Yazyev, R. Cammi, C. Pomelli, J.W. Ochterski, K.M.R.L. Martin, V.G. Zakrzewski, G.A. Voth, J.J.D.P. Salvador, S. Dapprich, A.D. Daniels, J.B.F.O. Farkas, J.V. Ortiz, J. Cioslowski, D.J. Fox, Revision B.01, Gaussian, Inc., Wallingford CT, 2009.
[52] F. Wang, W. Liu, Chem. Phys. 311 (2005) 63–69.
[53] A.S. Chaves, G.G. Rondina, M.J. Piotrowski, P. Tereshchuk, J.L.F. Da Silva, J. Phys. Chem. A 118 (2014) 10813–10821.
[54] I. Kei, T. Hiroto, A. Kazuhisa, J. Phys. B At. Mol. Opt. Phys. 40 (2007) 427.
[55] J. Wang, G. Wang, J. Zhao, Phys. Rev. A 68 (2003), 013201.
[56] G. Guzmán-Ramírez, F. Aguilera-Granja, J. Robles, Eur. Phys J. D 57 (2010) 49–60.